Journal of Scientific & Industrial Research
Vol. 81, December 2022, pp. 1285-1296
DOI: 10.56042/jsir.v81i12.48287

UAV Formation Control under Fixed and Variable Adjacency based Directed Network Topologies

Arindam Singha[1]*, Anjan Kumar Ray[1] & Arun Baran Samaddar[2]

[1]Department of Electrical and Electronics Engineering, National Institute of Technology Sikkim, Ravangla, South Sikkim 737 139, India

[2]National Institute of Technology Sikkim, Ravangla, South Sikkim 737 139, India

Received 01 April 2021; revised 07 November 2022; accepted 08 November 2022

The UAV formation control is one of the key aspects in several applications like surveillance, moving target tracking, load-transportation, and delivery systems etc. These situations demand the multiple UAVs to manoeuvre in a desired formation. To address this problem, a distributed formation control scheme is proposed incorporating the details about the state of the neighbouring UAVs. The communication network topology among the UAVs is considered to be directed with the constant and the weighted adjacency matrices. The nonholonomic constraints are considered while deriving the desired Euler angles. Satisfying the conditions of Lyapunov provides necessary proof of stability along the positional and the attitude subsystems. Simulation results demonstrate that the desired tetrahedron, octahedron, and cube shapes are attained and maintained by the UAVs successfully. Also, the designed formation paradigm works proficiently for both the constant and the weighted adjacency matrices based directed network topologies. The performance validation is done through extensive comparative analysis for varying network connections.

Keywords: Graph network, Laplacian matrix, Lyapunov stability, Nonholonomic constraints, Weighted adjacency matrix

Introduction

In recent times, the applications of Unmanned Aerial Vehicle (UAV) have been increased due to its wide area of applications. Instead of using a single UAV, the researchers are focusing on developing controller for multi-UAV system as it provides certain flexibility and advantages. A few important real-time applications of multi-UAV system in both the military and the civilian areas are surveillance[1], agriculture[2], target tracking[3], and load transportation[4] etc. The load transportation using multi-UAV system has applications in e-commerce delivery system also. In military applications, the multi-UAV system can be useful for monitoring of remote locations, or building a map of an unknown area. Surrounding a moving target with the help of multi-UAV fixed-wing system was shown in Sun *et al.*[3] The use of multi-UAV system in agricultural spraying was discussed in Hegde & Ghose.[4] A sliding mode controller based cooperative load-sharing between two UAVs was described in Rao *et al.*[5] Jang *et al.*[6] presented a detailed review on various cost-effective UAV platforms for field plant breeding. The multi-UAV system can also be applied to map a disaster-struck area.[7] Here, the authors applied the multiple heterogeneous UAV systems to map an area which was affected severely by earthquake/tsunami in Japan. The efficiency of the projected controller was assessed through multiple circumstances of map building. Moraes *et al.*[8] presented a multi-UAV control approach for real-time crowd monitoring where the UAVs were instructed to track the movement of a group of people. They had used auction paradigm to assign the target to any individual UAV and monitored the movement cooperatively. In Yu *et al.*[9], a time-varying formation control methodology was developed for forest fire monitoring cooperatively. One of the modern age applications of multi-UAV formation is e-commerce delivery. In Cokyasar *et al.*[10] presented an optimized control algorithm for e-commerce delivery through a drone system. In all those applications, the formation control of UAVs has taken a pivotal role.

Now, a formation controller might be functional in a decentralized or centralized manner. Another aspect of designing the controller is based on the network topological connections among UAVs which are directed[11–15] and undirected[16,17] network topologies. Several authors had designed formation controller

*Author for Correspondence
E-mail: arindamsingha008@gmail.com

based on the dynamic[18] or the kinematic models[19] of the UAVs. Each of these approaches had relative pros and cons. In dynamical model, controller needs to have complete information about the physical parameters of the UAVs. This complication is not present in kinematic model-based controller design. In directed network connection, the sending and receiving state information to the neighbouring UAVs is limited and depends upon the direction of the connection. In undirected network topology, the sharing of state information is not restricted where it solely depends on the communication range of the UAVs.

In Julian & Kochenderfer[1], the authors proposed a distributed controller for surveillance monitoring of wildfire using a fixed-wing aircraft. They used two deep reinforcement learning methods to accomplish the task. Back stepping controller driven distributed formation controllers were developed in Zhang *et al.*[12] & Kartal *et al*.[20] In Zhang *et al.*[12], the proposed controller worked on the leader-follower based approach. The authors used Lyapunov criterion to validate the stability of their developed formation controllers. The proposed formation controller in Kartal *et al*.[20] was developed based on time delayed system without considering the gyroscopic effect on the attitude subsystem. To cope up with unknown disturbances, an extended state observer based formation controller was developed in Zhang *et al*.[13] The state observer estimated and compensated the unknown disturbances to minimize the tracking error. In more advance situation, the desired formation needs to be varying with time to pursue the time-varying formation controllers[21–23] among multiple UAVs were developed. In He *et al.*[23], the authors considered the communication delay constraints while designing the formation controller. The formation control problem was also addressed for Autonomous Underwater Vehicles (AUVs) and heterogeneous systems.[24–27] The formation control among AUVs based on back stepping controller was proposed in Pang *et al*.[24] The design of formation controllers among Unmanned Ground Vehicles (UGV) and UAV were described in Rahimi & Naqshi[26] & Rabelo *et al*.[27] In Rabelo *et al*.[27], the automatic landing or take-off on/from a static or moving platforms were presented. The authors developed a cooperative formation controller to maintain the desired formation among heterogeneous agents and validated through experimental studies. A collision avoidance methodology of multiple aircraft system was described in Zhao *et al*.[28] Sliding mode control based design of formation controllers were described in Nair *et al.*[29] and Wang *et al.*[30] Genetic algorithm[31,32] based path planning and formation control of multi-UAV system was also described in the literature. To maintain the formation, the key aspect of this type of work is to maintain the network connectivity. Diwakar *et al.*[33], Chakraborty *et al.*[34], Saini *et al.*[35] & Wazid *et al.*[36] presented works related to secure IOT based network connections and applications related to UAVs. Diwakar *et al.*[33] discussed different methodologies of wireless network technologies along with advantages.

In the work of Rao *et al.*[5], the simulation results were given in a 2D framework, though that work could be potentially extended to a 3D framework. In Zhang *et al*.[12], the authors did not consider the effect of vortex and wind field on the system dynamic model. Also, the proposed work was not task-oriented. So, based on the collective knowledge from the existing literature, the subsequent aspects are introduced-

1. A distributed multi-UAV formation control paradigm is developed through the scope of this work.
2. The Lyapunov functions are designed to satisfy the stability of the controller.
3. The desired pitch and roll angles are derived while considering the nonholonomic constraints.
4. The network connectivity strength is substantiated over the properties of Laplacian matrix.
5. The adjacency matrix value is depending upon the distance between the UAVs.
6. The designed formation controller is authenticated over a number of simulation studies on both the constant and the weighted adjacency matrix based directed graph network topologies.
7. Through several formations as well as comparative studies the usefulness of the proposed controller is demonstrated.

The remaining part of the article is systematized as follows: section 2 illustrates the problem formulation of a multi-UAV system related to formation control and describes the basic notion of related graph theory. Section 3 describes the mathematical modelling of the UAV. Section 4 presents the distributed formation controller design through the directed network topology. Section 5 shows the effectiveness through comparative studies and several simulation results. The advantages and disadvantages along with the scope of future extension of this work are presented in section 6.

Problem Formulation

This work addresses the problem of comparative studies among multiple UAVs. The objective of this work is to drive all the UAVs in a predefined formation while maintaining the network connectivity. The effectiveness of the proposed controller is validated upon three different desired formations. The desired formations are tetrahedron shaped using 4 UAVs, octahedron shaped using 6 UAVs, and cube shaped using 8 UAVs. As mentioned earlier, the UAVs are connected through directed network topology. The directed network topology is explained in the context of graph theory in the next subsection.

Graph Theory

n numbers of UAVs presented in the multi-UAV system. The network connection is represented graphically as $\mathrm{g} = (v, e)$. Here, the nodes are represented as v, and each node reflects the UAV positions. e represents edges and it provides information between two nodes. So, $v = 1, 2, \ldots, n$ and $\mathrm{e} \in (v_i, v_j)\ \forall\ (v_i, v_j) \in v, \mathrm{i} \neq j$. The neighbor of the i^{th} UAV can be determined depending upon the Euclidean distance between the i^{th} and the j^{th} UAV. It should be $\|p_i - p_j\| \leq R$, where the communication range of the UAV is represented as R, and p_i and p_j represent the positions of the respective UAVs respectively. So, the neighbours of the i^{th} UAV can be determined if the following condition satisfies[37]

$$N_i = v_j(v_j, v_i) \in e \quad \ldots (1)$$

The Laplacian matrix is presented analogically as the difference between the degree and adjacency matrix of the multi-UAV system. The degree matrix holds the information of total number of connections and the adjacency matrix presents individual connections of the i^{th} UAV with other UAVs. If there is a directed edge between the i^{th} UAV to the j^{th} UAV, it signifies that information can be shared to j^{th} from i^{th} UAV. In such situation, $a_{ji} > 0$, otherwise $a_{ji} = 0$. In case of constant adjacency matrix based directed graph, if the directed connection exists then $a_{ji} = 1$. In Eq. (2), the degree matrix formulation is illustrated for the i^{th} UAV.

$$d_i(t) = \sum_{(j \neq i)=1}^{n} a_{ij}(t) \quad \ldots (2)$$

So, the Laplacian matrix is expressed as[19]

$$\mathrm{L} = \mathrm{D} - \mathrm{A} \quad \ldots (3)$$

The conditions for a stable and connected directed network for a multi-UAV system are described as follows.

1. The directed network topology must contain a spanning tree.[20]
2. The stability condition for the directed network topology is at least one eigenvalue of zero, and positive real parts for rest of the Eigenvalues.[12,37]

UAV Dynamic Model

Before the discussion on the dynamic model, the following assumptions are considered.

1. The UAV system can be presented as the attitude and the attitude subsystems.
2. The UAVs have rigid body system and homogeneous nature.
3. The roll (ϕ_{1_i}) and the pitch (θ_{1_i}) angles are restricted to $(-\frac{\pi}{2}, \frac{\pi}{2})$ and the yaw angle (ψ_{1_i}) is restricted to $(-\pi, \pi)$ for the i^{th} UAV.[39]
4. It is assumed that every UAV has at least one connecting path with other UAVs.
5. While designing the distributed formation controller, the collision and obstacle avoidance complications have not considered.

The position of the UAV system in inertia frame is denoted as $\mathrm{E} = [x_e, y_e, z_e]$ and in body-fixed frame denoted as $\mathrm{B} = [x_b, y_b, z_b]$, where x, y, z denote the UAV positions along respective axes. Euler angles of the UAV are represented respectively as ϕ, θ, and ψ. The position and velocity can be denoted in a combined form as $p_i = [x_{1_i}, y_{1_i}, z_{1_i}]'$ and $\dot{p}_i = [\dot{x}_{1_i}, \dot{y}_{1_i}, \dot{z}_{1_i}]'$ respectively. Similarly, the Euler angles and angular velocities can be represented as $\vartheta_i = [\phi_{1_i}, \theta_{1_i}, \psi_{1_i}]'$ and $\dot{\vartheta}_i = [\dot{\phi}_{1_i}, \dot{\theta}_{1_i}, \dot{\psi}_{1_i}]'$ respectively along i^{th} UAV. The positional and angular accelerations are defined as $\ddot{p}_i = [\ddot{x}_{1_i}, \ddot{y}_{1_i}, \ddot{z}_{1_i}]'$ and $\ddot{\vartheta}_i = [\ddot{\phi}_{1_i}, \ddot{\theta}_{1_i}, \ddot{\psi}_{1_i}]'$ respectively.

The schematic diagram of the UAV is depicted in Fig. 1. The mathematical representation of the system dynamical model mathematical represented in Eq. (4).[38,39]

$$\begin{cases} \ddot{x}_{1_i} = U_{x_i} \frac{U_{1_i}}{m} \\ \ddot{y}_{1_i} = U_{y_i} \frac{U_{1_i}}{m} \\ \ddot{z}_{1_i} = \frac{C_{\phi_{1_i}} C_{\theta_{1_i}}}{m} U_{1_i} - g \\ \ddot{\phi}_{1_i} = \dot{\theta}_{1_i} \dot{\psi}_{1_i} \left(\frac{I_y - I_z}{I_x}\right) - \frac{J_r}{I_x} \dot{\theta}_{1_i} \omega_i + \frac{l}{I_x} U_{2_i} \\ \ddot{\theta}_{1_i} = \dot{\phi}_{1_i} \dot{\psi}_{1_i} \left(\frac{I_z - I_x}{I_y}\right) + \frac{J_r}{I_y} \dot{\phi}_{1_i} \omega_i + \frac{l}{I_y} U_{3_i} \\ \ddot{\psi}_{1_i} = \dot{\phi}_{1_i} \dot{\theta}_{1_i} \left(\frac{I_x - I_y}{I_z}\right) + \frac{1}{I_z} U_{4_i} \end{cases} \quad \ldots (4)$$

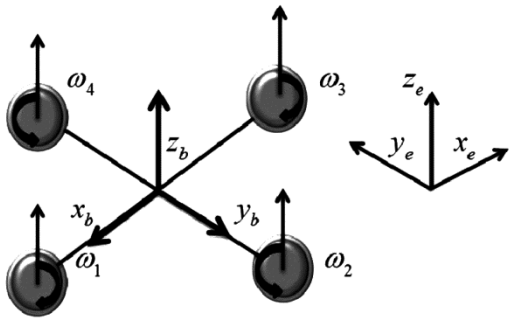

Fig. 1 — The UAV model

$U_{x_i} = C_{\phi_{1_i}} S_{\theta_{1_i}} C_{\psi_{1_i}} + S_{\phi_{1_i}} S_{\psi_{1_i}}$, and $U_{y_i} = C_{\phi_{1_i}} S_{\theta_{1_i}} S_{\psi_{1_i}} - S_{\phi_{1_i}} C_{\psi_{1_i}}$. The attitude subsystem contains the moment of inertia along 3 axes which are represented as I_x, I_y, and I_z respectively. The distance between the UAV and rotor center is denoted as l. J_r is the total moment of inertia. $\omega_i = \omega_{2_i} + \omega_{4_i} - \omega_{1_i} - \omega_{3_i}$, ω_i denotes speed of the i^{th} UAV rotor.[38] g stands for gravitational constant. The control input associated with positional subsystem is U_{1_i} and U_{2_i}, U_{3_i}, and U_{4_i} are the control inputs associated with the attitude subsystem.

Design of Distributed Formation Controllers

The design of formation controller along the translational and rotational motion is discussed in this section. The controller along positional subsystem of a UAV depends on the position and velocity of its neighbouring UAVs to reach the desired shape. The desired roll (ϕ) and pitch (θ) angles are derived for every UAVs individually considering the nonholonomic constraints.

Design of Controller for the Positional Subsystem

In the positional subsystem, the design of controller is explained along z-axis. Following the similar approach, the *x* and *y* axes controllers can also be designed. Let's consider, $\dot{z}_{1_i} = z_{2_i}$, so the modified dynamical model becomes

$$\ddot{z}_{1_i} = \dot{z}_{2_i} = \left(cos\phi_{1_i} cos\theta_{1_i}\right)\frac{U_{1_i}}{m} - g \quad \ldots (5)$$

$\dot{z}_{1_i}$ and $\ddot{z}_{1_i}$ denote the velocity and the acceleration. The difference between the actual and the desired position is defined as

$$e_{z_{1_i}} = z_{1_i} - z_{d_{1_i}} \quad \ldots (6)$$

The desired position is expressed as $z_{d_{1_i}}$. Now, the velocity error along the z-axis and its derivative can be written as

$$e_{z_{2_i}} = z_{2_i} - z_{d_{2_i}} \quad \ldots (7)$$

$$\dot{e}_{z_{2_i}} = \dot{z}_{2_i} - \dot{z}_{d_{2_i}} \quad \ldots (8)$$

$z_{d_{2_i}}$ is a virtual controller and it is defined as

$$z_{d_{2_i}} = \dot{z}_{d_{1_i}} - k_{z_{1_i}} e_{z_{1_i}} \quad \ldots (9)$$

The differentiation of $e_{z_{1_i}}$ is stated as follows after replacing $z_{d_{2_i}}$.

$$\dot{e}_{z_{1_i}} = e_{z_{2_i}} - k_{z_{1_i}} e_{z_{1_i}} \quad \ldots (10)$$

Now functions $e_{d_{z_{ij}}}$ and $\hat{e}_{z_i}$ are defined as

$$e_{d_{z_{ij}}} = \left|z_{1_i} - z_{1_j}\right| - \delta_{z_{ij}} \quad \ldots (11)$$

$$\hat{e}_{z_i} = e_{z_{2_i}} + e_{z_{1_i}} + \sum_{j \in N_i} a_{ij} e_{d_{z_{ij}}} \quad \ldots (12)$$

$\delta_{z_{ij}}$ and $e_{d_{z_{ij}}}$ are the desired displacement and relative desired positional error along z-axis between the i^{th} and the j^{th} UAVs. The control input U_{1_i} can be designed as

$$U_{1_i} = \frac{m}{cos\,\phi_{1_i} cos\,\theta_{1_i}}\left(-\dot{e}_{z_{1_i}} + \dot{z}_{d_{2_i}} + g - k_{z_{2_i}} sgn\left(\hat{e}_{z_i}\right) - \sum_{j \in N_i} a_{ij} \dot{e}_{d_{z_{ij}}}\right) \quad \ldots (13)$$

In the next subsection, the stability proof is given.

Proof of Stability of Controller along Positional Subsystem

The Lyapunov function is considered as

$$V_{z_i} = \frac{1}{2}\left(\hat{e}_{z_i}\right)^2 \quad \ldots (14)$$

The differentiation of Eq. (14) yields,

$$\begin{aligned} \dot{V}_{z_i} &= \left(\hat{e}_{z_i} \dot{\hat{e}}_{z_i}\right) \\ &= \hat{e}_{z_i}\left(\dot{e}_{z_{2_i}} + \dot{e}_{z_{1_i}} + \sum_{j \in N_i} a_{ij} \dot{e}_{d_{z_{ij}}}\right) \\ &= \hat{e}_{z_i}\left(\dot{z}_{2_i} - \dot{z}_{d_{2_i}} + \dot{e}_{z_{1_i}} + \sum_{j \in N_i} a_{ij} \dot{e}_{d_{z_{ij}}}\right) \end{aligned} \quad \ldots (15)$$

Substituting the value of $\dot{z}_{2_i}$ from Eq. (5), it yields

$$\dot{V}_{z_i} = \hat{e}_{z_i}\left(cos\,\phi_{1_i} cos\,\theta_{1_i} \frac{U_{1_i}}{m} - g - \dot{z}_{d_{2_i}} + \dot{e}_{z_{1_i}} + \sum_{j \in N_i} a_{ij} \dot{e}_{d_{z_{ij}}}\right) \quad \ldots (16)$$

Replacing U_{1_i} in Eq. (16), it becomes

$$\dot{V}_{z_i} = -k_{z_{2_i}} \left|\hat{e}_{z_i}\right| \quad \ldots (17)$$

While $k_{z_{1_i}}$ and $k_{z_{2_i}}$ are constants and greater than zero, then $\dot{V}_{z_i} \leq 0$. The system is asymptotic stable if the Lyapunov function is positive definite and its differentiation is negative definite. Henceforth, it is to mention that the designed formation controller is asymptotically stable. The control inputs U_{x_i} and U_{y_i} along x and y axes can be designed as

$$U_{x_i} = \frac{m}{U_{1_i}}\left(-\dot{e}_{x_{1_i}} + \dot{x}_{d_{2_i}} - k_{x_{2_i}} sgn(\hat{e}_{x_i}) - \sum_{j\in N_i} a_{ij}\dot{e}_{d_{x_{ij}}}\right) \quad \ldots (18)$$

$$U_{y_i} = \frac{m}{U_{1_i}}\left(-\dot{e}_{y_{1_i}} + \dot{y}_{d_{2_i}} - k_{y_{2_i}} sgn(\hat{e}_{y_i}) - \sum_{j\in N_i} a_{ij}\dot{e}_{d_{y_{ij}}}\right) \quad \ldots (19)$$

Desired Euler Angles

The inclusion of nonholonomic constraints signifies that the Euler angles do influence the movement of the UAV.[40] From Eqs (20) and (21), the desired roll and pitch angles can be determined for the i^{th} UAV respectively.[39] The desired yaw angle is constant $\psi_{d_{1_i}} = 0.7854\ (rad)$ for all UAVs.

$$\phi_{d_{1_i}} = sin^{-1}\left(U_{e_{x_i}} sin\psi_{1_i} - U_{e_{y_i}} cos\psi_{1_i}\right) \quad \ldots (20)$$

$$\theta_{d_{1_i}} = sin^{-1}\left(\frac{U_{e_{x_i}}}{cos\phi_{1_i} cos\psi_{1_i}} - \frac{sin\psi_{1_i} sin\phi_{1_i}}{cos\phi_{1_i} cos\psi_{1_i}}\right) \quad \ldots (21)$$

where, $U_{e_{x_i}}$ and $U_{e_{y_i}}$ are defined as

$$U_{e_{x_i}} = \frac{\left(\dot{x}_{d_i} - \dot{x}_{1_i}\right)m}{U_{1_i}} \quad \ldots (22)$$

$$U_{e_{y_i}} = \frac{\left(\dot{y}_{d_i} - \dot{y}_{1_i}\right)m}{U_{1_i}} \quad \ldots (23)$$

Design of Controller for the Attitude Subsystem

This section describes controller associated for pitch angle (θ_{1_i}). By following the similar method, the roll (ϕ_{1_i}) and the yaw angle (ψ_{1_i}) controllers can also be designed. Let $\theta_{2_i} = \dot{\theta}_{1_i}$, so the updated state dynamics is

$$\dot{\theta}_{2_i} = \dot{\phi}_{1_i}\dot{\psi}_{1_i}\left(\frac{I_z - I_x}{I_y}\right) + \frac{J_r}{I_y}\dot{\phi}_{1_i}\omega_i + \frac{l}{I_y}U_{3_i} \quad \ldots (24)$$

$\ddot{\theta}_{1_i}$ and $\dot{\theta}_{1_i}$ represent the angular acceleration and velocity respectively. The attitude error between the actual and the desired pitch angles is

$$e_{\theta_{1_i}} = \theta_{1_i} - \theta_{d_{1_i}} \quad \ldots (25)$$

Now, the velocity error $e_{\theta_{2_i}}$ along the pitch angle is defined as

$$e_{\theta_{2_i}} = \theta_{2_i} - \theta_{d_{2_i}} \quad \ldots (26)$$

$\theta_{d_{2_i}}$ is the virtual control which is designed as

$$\theta_{d_{2_i}} = \dot{\theta}_{d_{1_i}} - k_{\theta_{1_i}} e_{\theta_{1_i}} \quad \ldots (27)$$

where, $k_{\theta_{1_i}}$ is a constant and $k_{\theta_{1_i}} > 0$. The differential form of Eq. (25) after replacing the value of the virtual control is given as

$$\dot{e}_{\theta_{1_i}} = e_{\theta_{2_i}} - k_{\theta_{1_i}} e_{\theta_{1_i}} \quad \ldots (28)$$

The differentiation of the angular velocity error $e_{\theta_{2_i}}$ after replacing the derivative form of virtual control is given as

$$\dot{e}_{\theta_{2_i}} = \dot{\theta}_{2_i} - \ddot{\theta}_{d_{1_i}} + k_{\theta_{1_i}} \dot{e}_{\theta_{1_i}} \quad \ldots (29)$$

The Lyapunov based control input U_{3_i} is expressed as

$$U_{3_i} = \frac{I_y}{l}\left(-e_{\theta_{1_i}} + \ddot{\theta}_{d_{1_i}} - k_{\theta_{1_i}}\dot{e}_{\theta_{1_i}} - \dot{\phi}_{1_i}\dot{\psi}_{1_i}\left(\frac{I_z - I_x}{I_y}\right) - \frac{J_r}{I_y}\dot{\phi}_{1_i}\omega_i - k_{\theta_{2_i}} sgn\left(e_{\theta_{2_i}}\right)\right) \quad \ldots (30)$$

Proof of Stability of Controller along Attitude Subsystem

The stability is verified by satisfying the Lyapunov stability condition. Let's consider,

$$V_{\theta_i} = \frac{1}{2}\left(e_{\theta_{1_i}}\right)^2 + \frac{1}{2}\left(e_{\theta_{2_i}}\right)^2 \quad \ldots (31)$$

Derivative of Eq. (31) yields

$$\begin{aligned}\dot{V}_{\theta_i} &= \left(e_{\theta_{1_i}}\dot{e}_{\theta_{1_i}}\right) + \left(e_{\theta_{2_i}}\dot{e}_{\theta_{2_i}}\right)\\ &= e_{\theta_{1_i}}e_{\theta_{2_i}} - k_{\theta_{1_i}}e_{\theta_{1_i}}^2 + e_{\theta_{2_i}}\left(\dot{\theta}_{2_i} - \ddot{\theta}_{d_{1_i}} + k_{\theta_{1_i}}\dot{e}_{\theta_{1_i}}\right)\\ &= -k_{\theta_{1_i}}e_{\theta_{1_i}}^2 + e_{\theta_{2_i}}\left(e_{\theta_{1_i}} + \dot{\theta}_{2_i} - \ddot{\theta}_{d_{1_i}} + k_{\theta_{1_i}}\dot{e}_{\theta_{1_i}}\right)\end{aligned} \quad \ldots (32)$$

Replacing $\dot{\theta}_{2_i}$ in Eq. (32) yields

$$\dot{V}_{\theta_i} = -k_{\theta_{1_i}}e_{\theta_{1_i}}^2 + e_{\theta_{2_i}}\left(\phi_{1_i}\psi_{1_i}\left(\frac{I_z - I_x}{I_y}\right) + \frac{l}{I_y}U_{3_i} + \frac{J_r}{I_y}\dot{\phi}_{1_i}\omega_i + e_{\theta_{1_i}} - \ddot{\theta}_{d_{1_i}} + k_{\theta_{1_i}}\dot{e}_{\theta_{1_i}}\right) \quad \ldots (33)$$

Substituting U_{3_i} in Eq. (33) becomes,

$$\dot{V}_{\theta_i} = -k_{\theta_{1_i}}e_{\theta_{1_i}}^2 - k_{\theta_{2_i}}\left|e_{\theta_{2_i}}\right| \quad \ldots (34)$$

As $k_{\theta_{1_i}}$ and $k_{\theta_{2_i}}$ are positive constants, then $\dot{V}_{\theta_i} \leq 0$. Hence the proposed controller U_{3_i} provides an asymptotic stability along the pitch angle. The controller for the roll angle (U_{2_i}) and the yaw angle (U_{4_i}) can also be designed as

$$U_{2_i} = \frac{I_x}{l}\left(-e_{\phi_{1_i}} + \ddot{\phi}_{d_{1_i}} - k_{\phi_{1_i}}\dot{e}_{\phi_{1_i}} - \dot{\theta}_{1_i}\dot{\psi}_{1_i}\left(\frac{I_y - I_z}{I_x}\right) + \frac{J_r}{I_x}\dot{\theta}_{1_i}\omega_i - k_{\phi_{2_i}} sgn\left(e_{\phi_{2_i}}\right)\right) \quad \ldots (35)$$

$$U_{4_i} = I_z\left(-e_{\psi_{1_i}} + \ddot{\psi}_{d_{1_i}} - k_{\psi_{1_i}}\dot{e}_{\psi_{1_i}} - \dot{\phi}_{1i}\dot{\theta}_{1i}\left(\frac{I_x - I_y}{I_z}\right) - k_{\psi_{2_i}} sgn\left(e_{\psi_{2_i}}\right)\right) \quad \ldots (36)$$

Simulation Results

The competence of the designed control paradigm is demonstrated through multiple situations. The x, y, z coordinates of the target trajectory are as follows $x_t = 20 \times sin(0.1 \times t)$; $y_t = 20 \times cos(0.1 \times t)$; $z_t = 4 + (0.2 \times t)$ for all three situations. The parameter values used to simulate the proposed controller are taken from[41] and tabulated in Table 1. The desired trajectory for the first UAV is same as the target trajectory, the desired positions of the UAVs regarding the reference trajectory is given in Table 2. The controller gains are $k_{x_{1_i}} = k_{y_{1_i}} = k_{z_{1_i}} = k_{x_{2_i}} = k_{y_{2_i}} = k_{z_{2_i}} = k_{\phi_{1_i}} = k_{\theta_{1_i}} = k_{\psi_{1_i}} = 2$, and $k_{\phi_{2_i}} = k_{\theta_{2_i}} = k_{\psi_{2_i}} = 0.001$. The moment of inertia across propeller axis (J_r) is taken as $3.357 \times 10^{-5}\ kg.m^2$ and Fig. 2 depicts the desired structure with directed communication links for all three desired shape formations.

Table 1 — Parameter values of UAV[41,42]

Parameters	m(kg)	l(m)	g(m/s^2)	$I_x(kg.m^2)$	$I_y(kg.m^2)$	$I_z(kg.m^2)$
Values	0.5	0.2	9.81	4.85×10^{-3}	4.85×10^{-3}	8.81×10^{-3}

Table 2 — Position of target trajectory and the respective UAVs

Sl. No.	Desired shape	UAV positions	Parameter values
1	Tetrahedron shaped	$x_{1_1} = x_t, y_{1_1} = y_t, z_{1_1} = z_t$	
		$x_{1_2} = x_{1_1} + \frac{b}{2}, y_{1_2} = y_{1_1} + \mathrm{b}\frac{\sqrt{3}}{2}, z_{1_2} = z_{1_1}$	b = 4m
		$x_{1_3} = x_t - \frac{b}{2}, y_{1_3} = y_t + \mathrm{b}\frac{\sqrt{3}}{2}, z_{1_3} = z_{1_1}$	$\mathrm{s} = \mathrm{b} \times \left(\frac{\sqrt{3}}{2}\right)\mathrm{m}$
		$x_{1_4} = (x_{1_2} + x_{1_3})/2, y_{1_4} = \left((y_{1_2} + y_{1_3})/2\right) - \mathrm{s}/3$	$\mathrm{h} = \mathrm{b} \times \left(\frac{\sqrt{6}}{3}\right)\mathrm{m}$
		$z_{1_4} = (z_{1_2} + z_{1_3})/2 + \mathrm{h}$	
2	Octahedron shaped	$x_{1_1} = x_t, y_{1_1} = y_t, z_{1_1} = z_t$	
		$x_{1_2} = x_{1_1} + \mathrm{b}, y_{1_2} = y_{1_1}, z_{1_2} = z_{1_1}$	
		$x_{1_3} = x_{1_1}, y_{1_3} = y_{1_1} + \mathrm{b}, z_{1_3} = z_{1_1}$	b = 4m
		$x_{1_4} = x_{1_3} - \mathrm{b}, y_{1_4} = y_{1_3}, z_{1_4} = z_{1_1}$	$\mathrm{h} = \mathrm{b} \times \left(\frac{1}{\sqrt{2}}\right)\mathrm{m}$
		$x_{1_5} = (x_{1_1} + x_{1_3})/2, y_{1_5} = (y_{1_1} + y_{1_3})/2, z_{1_5} = z_{1_1} + \mathrm{h}$	
		$x_{1_6} = (x_{1_1} + x_{1_3})/2, y_{1_6} = (y_{1_1} + y_{1_3})/2, z_{1_6} = z_{1_1} - \mathrm{h}$	
3	Cube shaped	$x_{1_1} = x_t, y_{1_1} = y_t, z_{1_1} = z_t$	
		$x_{1_2} = x_{1_1}, y_{1_2} = y_{1_1} + \mathrm{b}, z_{1_2} = z_{1_1}$	
		$x_{1_3} = x_{1_1} + \mathrm{b}, y_{1_3} = y_{1_1} + \mathrm{b}, z_{1_3} = z_{1_1}$	
		$x_{1_4} = x_{1_1} + \mathrm{b}, y_{1_4} = y_{1_1}, z_{1_4} = z_{1_1}$	
		$x_{1_5} = x_{1_1}, y_{1_5} = y_{1_1}, z_{1_5} = z_{1_1} + \mathrm{b}$	b = 4m
		$x_{1_6} = x_{1_1}, y_{1_6} = y_{1_1} + \mathrm{b}, z_{1_6} = z_{1_1} + \mathrm{b}$	
		$x_{1_7} = x_{1_1} + \mathrm{b}, y_{1_7} = y_{1_1} + \mathrm{b}, z_{1_7} = z_{1_1} + \mathrm{b}$	
		$x_{1_8} = x_{1_1} + \mathrm{b}, y_{1_8} = y_{1_1}, z_{1_8} = z_{1_1} + \mathrm{b}$	

Tetrahedron Shaped Formation

Achieving and maintaining tetrahedron shaped formation with four UAVs is shown here. Through Table 3 the initial position and angle of an individual UAV is presented. The value of communication range R is taken as 6m in this case. The entire trajectories along with their positions at time $0s, 7s,$ and $25s$ are depicted in and maintained the anticipated formation. The illustration of the positional errors of the UAVs is given in Fig. 4(a). The angular errors along respective angles are shown in Fig. 4(b). So, it is to be mentioned that with the help of designed controller the positional and angular errors converge toward zero.

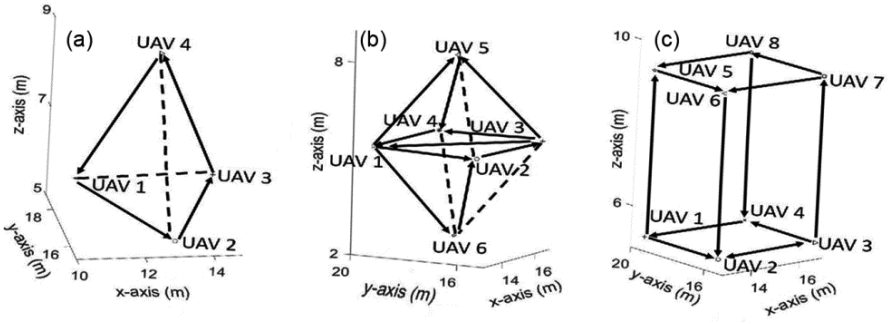

Fig. 2 — Desired formations with a directed communication topology: (a) tetrahedron; (b) octahedron; and (c) cube

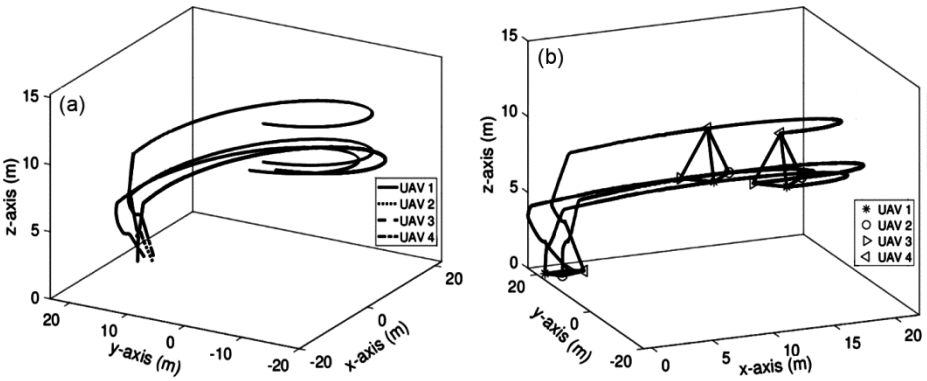

Fig. 3 — Tetrahedron shaped formation: (a) Entire trajectories, and (b) positions at different time

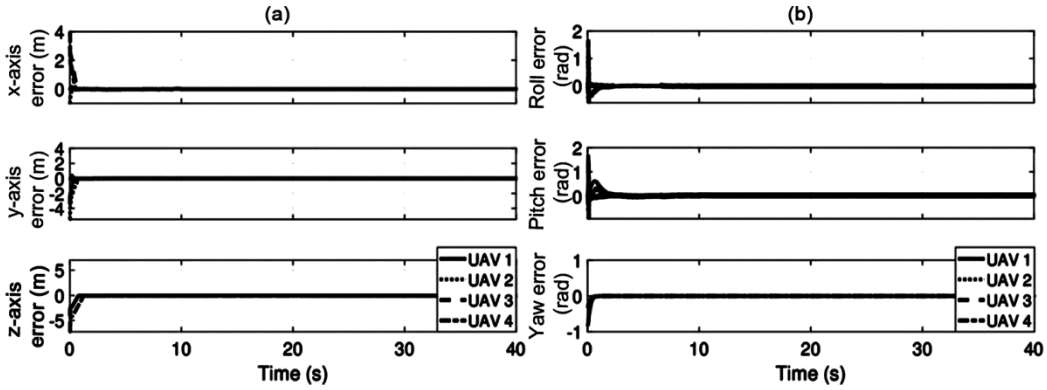

Fig. 4 — Tetrahedron shaped formation: (a) positional errors, and (b) attitude errors

Table 3 — Tetrahedron shaped formation: UAV initial positions and angles

Initial values	UAV 1	UAV 2	UAV 3	UAV 4
Position	(0, 20, 0)	(1, 18, 0)	(2, 20, 0)	(3, 19, 0)
Angle	(0, 0, 0)	(0, 0, 0.5)	(0, 0, 0.5)	(0, 0, 0.5)

Octahedron Shaped Formation

The octahedron shaped desired formation with six UAVs is presented in this section. The UAVs' starting positions and angles are specified in Table 4. The value of communication range R is taken as $8m$ in this case. In Fig. 5(a), it is showed that the UAVs have successfully achieved octahedron formation while tracking respective trajectories. UAV positions at time $0s, 7s$, and $25s$ in Fig. 5(b). It depicts that the UAVs are initially placed without a formation structure, nevertheless the desired formation is accomplished and preserved with the help of the proposed formation controller. The positional and attitude errors of the UAVs are shown in Figs. 6(a) and 6(b) respectively. The positional and attitude errors of all UAVs converge towards zero.

Cube Shaped Formation

In this case, eight UAVs are instructed to form a cube shaped formation. The value of communication range parameter (R) of the UAV is considered as 8m. The starting positions and angles of the UAVs are given in Table 5. The trajectory and UAV positions at different time sample are depicted in Fig. 7(a) and 7(b) respectively. The positional and attitude errors of the UAVs are depicted in Fig. 8(a) and Fig. 8(b) respectively.

Weighted Adjacency Based Directed Network Topology

This section shows the formation control result for the weighted adjacency matrix based directed graph network topology. The initial conditions are same for all the UAVs as mentioned earlier. The process of calculating the weighted adjacency matrix is described as[19]

$$a_{ij} = e^{\left(-\frac{\eta}{R}\|p_i - p_j\|\right)} \quad \ldots (37)$$

where, η is a positive constant value. The value of η is taken as 5. It is conclusive that, in this case, the

Table 4 — Octahedron shaped formation: UAV initial positions and angles

Initial values	UAV 1	UAV 2	UAV 3	UAV 4	UAV 5	UAV 6
Position	(0, 22, 2)	(−1, 20, 1)	(4, 18, 3)	(3, 20, 3)	(−5, 25, 2)	(4, 26, 1)
Angle	(0, 0, 0)	(0, 0, 0.5)	(0, 0, 0.5)	(0, 0, 0.5)	(0, 0, 0.5)	(0, 0, 0.5)

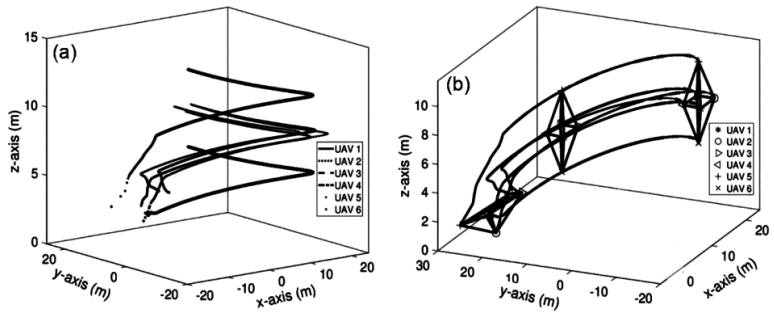

Fig. 5 — Octahedron shaped formation: (a) Entire trajectories, and (b) positions at different time

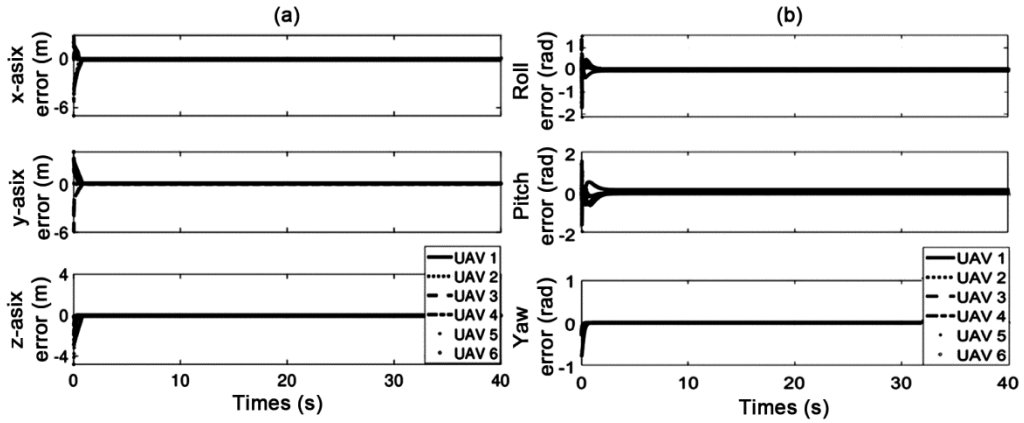

Fig. 6 — Octahedron shaped formation: (a) positional errors, and (b) attitude errors

Table 5 — Cube shaped formation: UAV initial positions and angles

Initial values	UAV 1	UAV 2	UAV 3	UAV 4	UAV 5	UAV 6	UAV 7	UAV 8
Position	(0, 22, 2)	(−1, 20, 1)	(4, 18, 3)	(3, 20, 3)	(−5, 25, 2)	(4, 26, 1)	(−4,21, 1.5)	(−4, 20, 3)
Angle	(0, 0, 0)	(0, 0, 0.5)	(0, 0, 0.5)	(0, 0, 0.5)	(0, 0, 0.5)	(0, 0,0.5)	(0, 0, 0.5)	(0, 0, 0.5)

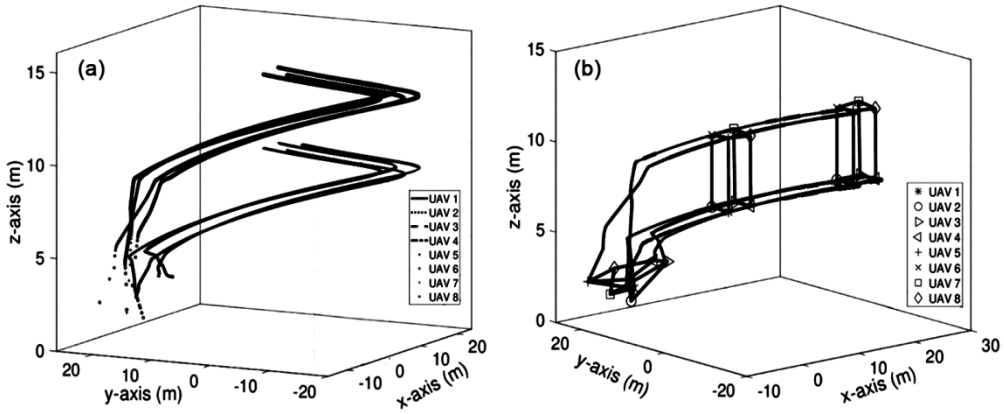

Fig. 7 — Cube shaped formation: (a) Entire trajectories, and (b) positions at different time

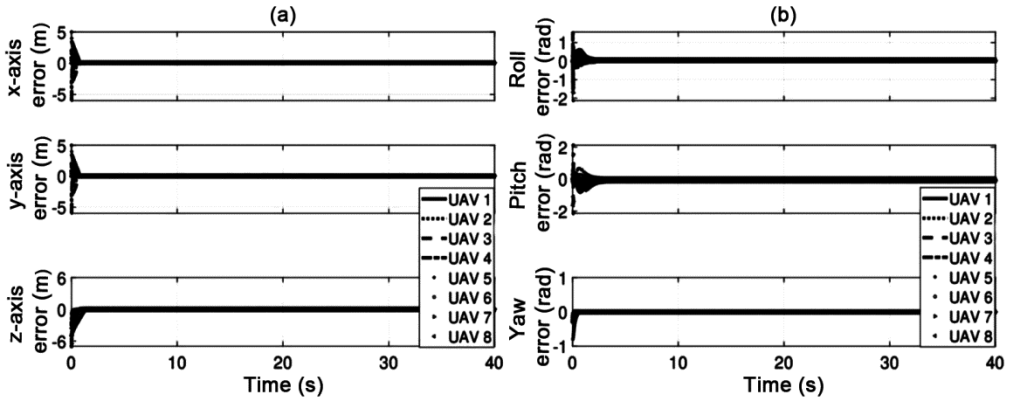

Fig. 8 — Cube shaped formation: (a) positional errors, and (b) attitude errors

value of the adjacency matrix is depending upon the communication range as well as distance between the i^{th} and the j^{th} UAVs. A comparative result between the constant and the weighted adjacency matrix based directed communication topology is tabulated in Table 6 with respect to the root mean square error (RMSE) for all three situations of every UAV. The combined errors of x, y, and z axes are taken for positional RMSE and ϕ, θ, and ψ angles are taken for attitude RMSE. The results signify that despite of the variation in the communication topology, the proposed formation controller performs satisfactorily.

Comparative Study and Discussion

The comparative analysis is performed with articles [43,18] to demonstrate its effectiveness. In Li *et al.*[43], the multi-UAV system has 4 UAVs (1 leader and 3 followers). To perform the comparative study, the initial conditions and parameter values are kept as same as in Li *et al.*[43] for the follower UAVs. The control inputs are also designed in the paper in line of the dynamic model presented in Li *et al.*[43] The effectiveness of the controllers is compared with respect to the settling time taken by each follower UAVs. The comparative result is tabulated in Table 7. In Li *et al.*[43], the errors along x, y, and z axes settled near $9s$. Whereas, using the proposed formation controller the positional errors settled within $5s$. Along attitude subsystem, the proposed controller performs better than the controller proposed in Li *et al.*[43] In Zhao *et al.*[18], the system consists of 6 followers and 1 leader UAV and communicating

Table 6 — RMSE values for constant and weighted adjacency matrix based directed communication topology

Desired formation	UAVs	Directed topology		Weighted directed topology	
		Positional error (m)	Attitude error (rad)	Positional error (m)	Attitude error (rad)
Tetrahedron	UAV 1	0.3147	0.0965	0.1955	0.0814
	UAV 2	0.3578	0.0766	0.3247	0.0995
	UAV 3	0.3793	0.0835	0.3083	0.0851
	UAV 4	0.6082	0.0836	0.4798	0.0661
Octahedron	UAV 1	0.5228	0.3404	0.1298	0.0892
	UAV 2	0.6113	0.3576	0.3123	0.0923
	UAV 3	0.3470	0.1918	0.3529	0.1289
	UAV 4	0.3400	0.1482	0.2440	0.1006
	UAV 5	0.4923	0.1827	0.5139	0.1516
	UAV 6	0.3474	0.1560	0.2167	0.0725
Cube	UAV 1	0.1523	0.0798	0.1177	0.0734
	UAV 2	0.2705	0.0890	0.2440	0.0862
	UAV 3	0.3957	0.1231	0.3542	0.1282
	UAV 4	0.2099	0.0947	0.0979	0.0659
	UAV 5	0.5841	0.1620	0.5152	0.1327
	UAV 6	0.5534	0.1393	0.4883	0.0758
	UAV 7	0.7108	0.1231	0.6583	0.1134
	UAV 8	0.6812	0.1317	0.5844	0.1344

Table 7 — Comparative analysis with[43] with respect to settling time

Controller	UAV	x_1	y_1	z_1	ϕ_1	θ_1	ψ_1
Proposed	UAV 1	4.950	1.073	3.255	0	0	0.172
	UAV 2	0.467	0.944	2.175	0	0	0.171
	UAV 3	3.883	0.881	1.478	0	0	0.172
Controller proposed in[43]	UAV 1	8.456	9.005	8.352	0	0	3.981
	UAV 2	8.651	8.902	8.507	0	0	3.474
	UAV 3	8.618	9.013	8.960	4.212	4.395	3.981

Table 8 — Comparison with[18] in terms of Mean error, MSE and MAE of the follower UAVs

Controller	Parameter	Mean	MSE	MAE
Proposed	X	$-2.162 * 10^{-4}$	$3.288 * 10^{-4}$	0.0427
	Y	$4.312 * 10^{-4}$	$3.340 * 10^{-4}$	0.0425
	Z	$1.87 * 10^{-5}$	$2.975 * 10^{-4}$	0.0422
	ϕ	0	0	0
	θ	0	0	0
	ψ	0	0	0
Controller proposed in[18]	X	$7.793 * 10^{-4}$	$2.941 * 10^{-4}$	0.014
	Y	$-1.287 * 10^{-4}$	$5.651 * 10^{-4}$	0.021
	Z	$9.849 * 10^{-4}$	$1.929 * 10^{-5}$	$9.880 * 10^{-4}$
	ϕ	$-6.231 * 10^{-4}$	$3.715 * 10^{-4}$	0.014
	θ	$-1.048 * 10^{-4}$	$5.056 * 10^{-4}$	0.015
	ψ	$-1.464 * 10^{-4}$	$1.330 * 10^{-5}$	$3.100 * 10^{-4}$

through the weighted adjacency based directed network topology. The follower UAVs were moving in a spiral trajectory and making a circular shaped formation. The proposed formation controller is modified according to the dynamic model presented in Zhao *et al.*[18] Similar values are taken for all parameters, initial conditions, and weighted adjacency matrix. In Table 8, the detailed quantitative comparative result in terms of the mean error, the mean square error (MSE), and the mean absolute error

(MAE) of all follower UAVs is presented. As the desired and initial yaw angles are same for all follower UAVs, the formation controller provides 0 mean error, MSE, and MAE along the yaw angle. As the initial ϕ and θ angles are zero, it results to zero desired roll and pitch angle. So, the mean error, MSE, and MAE along the roll and the pitch angles are observed to be 0 throughout the time for all follower UAVs. The mean error, MSE and MAE along x, y, and z axes are also satisfactory with respect to the controller developed by Zhao *et al*.[18] So, it is to be mentioned that the proposed distributed formation controller provides efficient results and works satisfactorily on different dynamical models too.

Conclusions

A control paradigm of a multi-UAV system is discussed in this paper for formation control. The proposed controller is asymptotically stable and the proof is provided through satisfying conditions of Lyapunov criteria. The communication network among UAVs is represented through the constant and the weighted adjacency matrices based directed graph topologies. In weighted adjacency matrix, the distance between the UAVs also influences the adjacency matrix calculation and in control input design. The proposed distributed formation controller is validated through varying numbers of the UAVs to achieve and maintain different desired shape of formations. Simulation results illustrate that the proposed formation controller works satisfactorily. The comparative study is also presented for both the directed and the weighted directed communication topologies and it is observed that it performs satisfactorily over other controllers for the same initial conditions. The potential scope of improvement is to develop a robust formation controller while the effect of disturbance is unknown on the system's dynamical model. The efficiency of the proposed formation controller can be tested through switching network topology-based connection where the type of the topology among the UAVs changes from undirected to directed and vice-versa as per the application. The proposed controller is asymptotically stable. The further scope of extension is to propose a finite-time formation controller. Finally, this work can be extended to implement on the hardware system.

Acknowledgement

This work was supported by the Visvesvaraya Ph.D. Scheme, Digital India Corporation (formerly known as the Media Lab Asia) for the project entitled "Intelligent Networked Robotic Systems".

References

1 Julian K D & Kochenderfer M J, Distributed wildfire surveillance with autonomous aircraft using deep reinforcement learning, *J Guid Control Dyn*, **42(8)** (2019) 1768–1778.

2 Izmaylov A Y, Smirov I, Kolesnikova V & Marchenko L, Substantiation of parameters of unmanned aerial vehicles for pesticides and fertilizers application in precision farming system, *Mech agric Conserv resour*, **63(5)** (2017) 168–170.

3 Sun Z, Garcia D M H, Anderson B D & Yu C, Collaborative target-tracking control using multiple fixed-wing unmanned aerial vehicles with constant speeds, *J Guid Control Dyn*, **44(2)** (2021) 238–250.

4 Hegde A & Ghose D, Multi-UAV distributed control for load transportation in precision agriculture, *AIAA Scitech Forum* 2020, 2068.

5 Rao S, Chakravarthy A & Ghose D, Planar manipulation of an object by unmanned aerial vehicles using sliding modes, *J Guid Control Dyn*, **44(1)** (2021) 120–137.

6 Jang G, Kim J, Yu J K, Kim H J, Kim Y, Kim D W & Chung Y S, Cost-effective unmanned aerial vehicle (UAV) platform for field plant breeding application, *Remote Sens*, **12(6)** (2020) 998.

7 Aljehani M & Inoue M, Performance evaluation of multi-UAV system in post-disaster application: Validated by HITL simulator, *IEEE Access*, **7** (2019) 64386–64400.

8 De-Moraes R S & De-Freitas E P, Multi-UAV based crowd monitoring system, *IEEE Trans Aerosp Electron Syst*, **56(2)** (2019) 1332–1345.

9 Yu Z, Zhang Y, Jiang B & Yu X, Fault-tolerant time-varying elliptical formation control of multiple fixed-wing UAVs for cooperative forest fire monitoring, *J Intell Rob Syst*, **101(3)** (2021) 1–15.

10 Cokyasar T, Optimization of battery swapping infrastructure for e-commerce drone delivery, *Comput Commun*, **168** (2021) 146–154.

11 Zhu X, Zhang X X & Qu Y H, Consensus-based three-dimensional multi-UAV formation control strategy with high precision, *Front Inf Technol Electron Eng*, **18(7)** (2017) 968–977.

12 Zhang J, Yan J & Zhang P, Multi-UAV formation control based on a novel back-stepping approach, *IEEE Trans Veh Technol*, **69(3)** (2020) 2437–2448.

13 Zhang B, Sun X, Liu S, & Deng X, Formation control of multiple UAVs incorporating extended state observer-based model predictive approach, *Int J Aeronaut Space Sci*, **20(4)** (2019) 953–963.

14 Zhang J, Wang W, Zhang Z, Luo K & Liu J. Cooperative control of UAV cluster formation based on distributed consensus, *IEEE* 15^{th} *Int Conf Cntrl Autom (ICCA)* (IEEE) 2019, 788–793.

15 Zhang B, Sun X, Liu L & Deng X, Adaptive differential evolution-based distributed model predictive control for multi-UAV formation flight, *Int J Aeronaut Space Sci*, **21** (2019) 538–548.

16 Ju C & Son H L, A distributed swarm control for an agricultural multiple unmanned aerial vehicle system, *Proc Inst Mech Eng I*, **233(10)** (2019) 1298–1308.

17 Singha A, Ray A K & Samaddar A B, Leader–follower based formation controller design for quadrotor UAVs, *Trans Indian Natl Acad Eng*. 7 (2022) 325–338.

18 Zhao Z, Wang J, Chen Y & Ju S, Iterative learning-based formation control for multiple quadrotor unmanned aerial vehicles, *Int J Adv Rob Syst*, **17(2)** (2020) 1729881420911520.

19 Dutta R, Sun L & Pack D, A decentralized formation and network connectivity tracking controller for multiple unmanned systems, *IEEE Trans Control Syst Technol*, **26(6)** (2017) 2206–2213.

20 Kartal Y, Subbarao K, Gans N R, Dogan A & Lewis F, Distributed backstepping based control of multiple UAV formation flight subject to time delays, *IET Control Theory Appl*, **14(12)** (2020) 1628–1638.

21 Zhang W, Chaoyang D, Maopeng R & Yang L, Fully distributed time-varying formation tracking control for multiple quadrotor vehicles via finite-time convergent extended state observer, *Chin J Aeronaut*, **33(11)** (2020) 2907–2920.

22 Xue R & Cai G, Formation flight control of multi-UAV system with communication constraints, *J Aerosp Technol Management*, **8(2)** (2016) 203–210.

23 He L, Zhang J, Hou Y, Liang X & Bai P, Time-varying formation control for second-order discrete-time multi-agent systems with directed topology and communication delay, *IEEE Access*, **7** (2019) 33517–33527.

24 Pang S, Wang J, Liu J & Yi H, Three-dimensional leader–follower formation control of multiple autonomous underwater vehicles based on line-of-sight measurements using the back stepping method, *Proc Inst Mech Eng I*, **232(7)** (2018) 819–829.

25 Mei F, Wang H, Yao Y, Fu J, Yuan X & Yu W, Robust second-order finite-time formation control of heterogeneous multi-agent systems on directed communication graphs, *IET Control Theory Appl*, **14(6)** (2020) 816–823.

26 Rahimi R, Abdollahi F & Naqshi K, Time-varying formation control of a collaborative heterogeneous multi agent system, *Rob Auton Syst*, **62(12)** (2014) 1799–1805.

27 Rabelo M F S, Brandao A S & Sarcinelli F M, Landing a UAV on static or moving platforms using a formation controller, *IEEE Syst J*, (2020) 1–9.

28 Zhao P, Wang W, Ying L, Sridhar B & Liu Y, Online multiple-aircraft collision avoidance method, *J Guid Control Dyn*, **43(8)** (2020) 1456–1472.

29 Nair R R, Behera L, Kumar V & Jamshidi M, Multi satellite formation control for remote sensing applications using artificial potential field and adaptive fuzzy sliding mode control, *IEEE Syst J*, **9(2)** (2014) 508–518.

30 Wang Z, Fei Q & Wang B, Distributed adaptive sliding mode formation control for multiple unmanned aerial vehicles, *Chin Cntrl Decision Conf (CCDC)* 2020, 2105–2110.

31 Liu Y, Qi N, Yao W, Zhao J & Xu S, Cooperative path planning for aerial recovery of a UAV swarm using genetic algorithm and homotopic approach, *Appl Sci*, **10(12)** (2020) 4154.

32 Najm A A, Ibraheem I K, Azar A T & Humaidi A J, Genetic optimization-based consensus control of multi-agent 6-DoF UAV system, *Sensors*, **20(12)** (2020) 3576.

33 Diwakar M, Singh P, Kumar P, Tiwari K & Bhushan S, A critical review on secure authentication in wireless network, *Lecture Notes in Electrical Engineering* (Springer) **768**, (2022).

34 Chakraborty A, Jindal M, Khosravi M R, Singh P, Shankar A & Diwakar M, A secure IoT-based cloud platform selection using entropy distance approach and fuzzy set theory, *Wirel Commun Mob Comput*, **2021** (2021).

35 Saini D K J B, Patil P, Gupta K D, Kumar S, Singh P & Diwakar M, Optimized web searching using inverted indexing technique, In *IEEE 11th Int Conf Commun Syst Netw Technol (CSNT)* (IEEE) 2022, 351–356.

36 Wazid M, Bera B, Mitra A, Das A K & Ali R, Private blockchain-envisioned security framework for AI-enabled IoT-based drone-aided healthcare services, In *Proc of the 2nd ACM MobiCom Workshop on Drone Assisted Wireless Communications for 5G and Beyond* (IEEE) 2020, 37–42.

37 Chen L, Li C, Sun Y & Ma G, Distributed finite-time tracking control for multiple uncertain Euler–Lagrange systems with input saturations and error constraints, *IET Control Theory Appl*, **13(1)** (2018) 123–133.

38 Basri M A M, Design and application of an adaptive backstepping sliding mode controller for a six-DoF quadrotor aerial robot, *Robotica*, **36(11)** (2018) 1701–1727.

39 Singha A, Ray A K & Samaddar A B, UGV-UAV coordination: Takeoff, landing and formation control, In *IEEE World Autom Congr (WAC)* (IEEE) 2021, 302–307.

40 Elhennawy A M & Habib M K, Trajectory tracking of a quadcopter flying vehicle using sliding mode control, 43^{rd} *Annual Conf of the IEEE Industrial Electronics Society* (IEEE) 2017, 6264–6269.

41 Bouzid Y, Bestaoui Y, Siguerdidjane H & Zareb M, Quadrotor guidance-control for flight like nonholonomic vehicles, *IEEE Int Conf Unmanned Aircraft Systems* (ICUAS) 2018, 980–988.

42 Basri M A M, Husain A R & Danapalasingam K A, Enhanced backstepping controller design with application to autonomous quadrotor unmanned aerial vehicle, *J Intell Rob Syst*, **79(2)** (2015) 295–321.

43 Li Y, Yang J & Zhang K, Distributed finite-time cooperative control for quadrotor formation, *IEEE Access*, **7** (2019) 66753–66763.